Proceedings of the
Annual Stability Conference
Structural Stability Research Council
Atlanta, Georgia, April 21-24, 2026

Buckling Behaviour of Additively Manufactured Equal Slender Unequal Leg Angles

Vijaya Vengadesh Kumar Jeyapragasam[1]

Abstract

Cold-formed steel members are fabricated from thin sheets, resulting in uniform element thickness throughout the cross-section. The slenderness of the element is primarily determined by its width for the specified sheet thickness. The additive manufacturing process enables 3D metal printing with specified cross-section dimensions. This 3D metal-printing technique enables independent element thicknesses within a cross-section. Hence, the slenderness of the element (width to thickness ratio) can be handled by modifying both the width and thickness within the cross-section. This presents an opportunity to print sections characterized by equal slenderness while varying in width and thickness.

This article numerically investigates the local buckling capacity of 3D metal printed angle sections having equal slender legs with independent element width and thickness. The 316L stainless steel angle sections are analyzed using ABAQUS. The influence of element geometry on the buckling is assessed through the evaluation of inter-element interactions. This novel study aims to expand the application of the Direct Strength Method of design to the general thin-walled sections with independent element thicknesses, achievable through the welding of elements with different thicknesses or via 3D metal printing techniques.

1. Introduction

The Direct Strength Method (DSM) is proven as the best design method for Cold-Formed Steel (CFS) columns, beams, and beam-column members, which utilizes the elastic critical buckling load obtained from the signature curve and the semi-empirical design equations to determine the capacity of the member. As the gross-section properties are sufficient and inter-element interactions are accounted for in elastic critical buckling load calculations, the DSM results yield simple calculations and realistic member behavior [Rasmussen, K.J.R. 2006]. The extension of DSM to different thicknesses and yield stresses within the cross-section elements is possible for welded members, but remains unexplored. However, welded members may affect member behavior due to hybrid material yield strength, heat-affected zone, residual stress, imperfections, and electrode material properties. These parameters make it difficult to isolate the geometrical influence of thin-walled members. Metal 3D printing eliminates the complications of the heat-affected zone, maintains the material as close to a homogeneous, isotropic nature, and, at the same time, maintains the required geometry of the cross-section with different element thicknesses.

[1] Assistant Professor, National Institute of Technology Karnataka - India, <vj@nitk.edu.in>

A comprehensive numerical study on inter-element interaction of plain channel with different element thicknesses is reported for various combinations of element slenderness in [Francis.R et al., 2024 and Francis.R et al., 2025]. The simple plate buckling equation does not account for the inter-element interaction; (a) when the aspect ratio (height to width ratio) of the plain channel cross-section equals to 3.05 for equal thickness elements, simultaneous buckling of unstiffened flanges and flange stiffened web will lower the local buckling capacity, and (b) at the same time, the element slenderness also involved in the post-local buckling strength with considerable strength enhancement, when one of the elements (web or flanges) are having non-slender elements. It shows the need for multiple DSM local buckling strength curves accounting for the aspect ratio of the section [Kumar, M. V. A et al., 2013, and Mahar, A. M. et al., 2021] and the element slenderness ratio to account for both the unfavorable effect of aspect ratio and the favorable effect of non-slender elements. The cross-section behavior of additively manufactured members are reported in [Buchanan, C. et al., 2017, Huang, C., et. al., 2022, Chen, Gardner., L., 2023, and Evans, S.I et. al., 2024].

These studies demonstrate that there is a clear scope to improve the DSM to account for the width-to-thickness ratios of stiffened and unstiffened elements in the local buckling strength enhancement of plain channels, along with the aspect ratio, which reduces strength due to simultaneous local buckling of elements. To understand the influence of inter-element interaction among unstiffened elements within a cross-section, the current study focuses on angle sections, with the element slenderness ratio (width-to-thickness ratio) as the main parameter.

In this article, angle sections with two unstiffened elements are studied numerically using the experimentally determined stress-strain curve for 3D-printed 316L-grade stainless steel coupons. The influence of the width-to-thickness ratio on the elastic critical buckling load and ultimate strength is examined, and interesting conclusions are summarized.

2. Material Strength Evaluation

3D metal printing uses different methods of material deposition, mainly the high-precision Laser Powder Bed Fusion (LPBF), the very fast Wire Arc Additive Manufacturing (WAAM), and the intermediate between these two, the Laser Direct Energy Deposition (L-DED). Among these three methods, the LPBF technique was used to print two metal coupons. Using 316L metal powder, the coupons were built layer by layer by melting the powder with alternating laser beams in longitudinal and cross-diagonal directions. The dimensions of the printed coupons, as per the ASTM standard, are presented in Fig. 1. The printed coupons were tested using a 25 kN MTS Universal Testing Machine available at the Central Research Facility, NITK Surathkal. The coupons are not extracted from the member; rather, they are printed directly using LPBF. Hence, the bending residual stress developed within the member is not implicitly accounted for in the coupon test. The membrane residual stress could be significant in LPBF due to the heating of alternating layers of metal powder, which creates a thermal gradient along the thickness of the printed elements. Hence, the material coupon test does not fully account for the residual stress involved, and a more detailed study of residual stress is required.

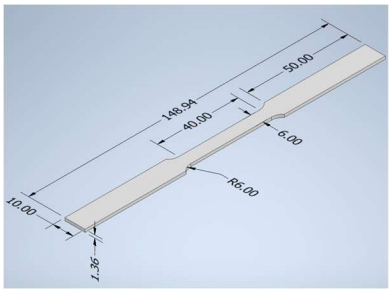

Figure 1: Coupon Dimension in mm

The average material properties of LPBF 3D printed coupons and general austenitic stainless steel of 316L are presented in Table 1. For the austenitic stainless steel grade, the Young's modulus (E) is slightly lower than that of mild steel. Interestingly, the proportional yield (Fy) and ultimate (Fu) strengths of the LPBF-printed materials are much higher than those of conventional 316L austenitic stainless steel. These properties are mainly influenced by the process parameters and the 3D printing technique used. In LPBF, the 45-micron spherical metal powder is melted and solidified to form 40-micron-thick layers. Hence, it slowly prints the member with an improved microstructure compared to traditional austenitic stainless steel [Shamsujjoha, M. et. al., 2018, Yin, Y.J. et al., 2019, Xu, M. et al., 2023 and, Chepkoech et. al., 2024]. This increased yield and ultimate strength significantly affect the buckling mode and enable possible interactions between buckling modes and the post-buckling residual strength of the member. The performance of the material is significantly better with 3D-printed metal than with conventional metal. The WAAM material properties are presented in [Evans, S.I et. al., 2023]

Table 1: Material Properties

Specimen	E (N/mm^2)	F_y (N/mm^2)	F_u (N/mm^2)
316-LPBF	182453	534.93	660.78
316L	190000	260.00	570.00

3. Selection of Geometry

This study examines the influence of geometry on the ultimate local buckling capacity of angle sections with equal element slenderness but unequal legs in width and/or thickness. Hence, the involvement of element slenderness and the aspect ratio of the cross-section is carefully chosen for every cross-section. In total, 12 sets of cross-sections, each with 10, are analyzed numerically. The considered specimens in set 1 include the effect of equal element slenderness ratio of both web and flanges, for a constant width (40 mm) and various thicknesses of 0.8, 1.0, 1.2, 1.6, 1.8, 2, 3, 4, 5, and 6 mm. In the second set, the width of the specimen from set 1 was increased to 120 mm to account for the size effect, which is directly reflected in the element slenderness. The third, fourth, and fifth sets maintain the element slenderness, with one leg having a 40 mm width and thicknesses of 0.8, 1.0, and 1.2 mm, respectively. For the other leg, the width was maintained at 40 mm, and the thickness was varied to 0.8, 1.0, 1.2, 1.6, 1.8, 2, 3, 4, 5, and 6 mm across all 3 sets. Hence, the inter-element slenderness was varied to understand the buckling behavior.

Sixth set specimens have equal slenderness ratios for both elements. However, the first element slenderness was varied for a constant width of 40 mm with thicknesses of 0.8, 1.0, 1.2, 1.6, 1.8, 2, 3, 4, 5, and 6 mm, and the second element width varied in 5 mm increments from 25 to 65 mm. The respective thicknesses to maintain the same slenderness of the other element were

predetermined. Hence, both elements will have equal element slenderness with unequal element width.

Seventh, eighth, and ninth sets of specimens have the same width of 40 mm for one element, and the second element width varied in 5 mm increments from 25 to 65 mm. The thickness of element 1 was maintained constant at 0.8, 1.6, and 3.0 mm, respectively, for the sets, and the thickness of the second element varied to maintain the equal and constant element slenderness within each set. Accordingly, the element slenderness was maintained as 49.5, 24.5, and 12.8, respectively. The final three sets of tenth, eleventh, and twelfth have the same dimensions as sets seven to nine, except for the width of the second element. The second element thickness was varied from 0.8, 1.0, 1.2, 1.6, 1.8, 2, 3, 4, 5, and 6 mm, and the respective width of the second element was predetermined for each set. The length of the member was limited to three times the maximum dimension of the cross-section.

Set 1 and Set 6 have equal element slenderness for different widths with corresponding thickness in the second element of Set 6. However, their buckling strength and post-buckling strength are similar. Hence, the DSM does not require multiple curves for equal slender elements. The non-dimensional slenderness ratio determined using elastic critical buckling strength and yield stress could be sufficient to estimate the nominal capacity of the member. Asymmetry in geometry does not influence the behavior.

4. Numerical Study

The finite element model was developed in ABAQUS CAE using the nonlinear material model [Arrayago et. al., 2015] derived from the average of two experimental results. The 3D shell element model was used to extrude the member from the centerline dimensions of the cross-section, assuming sharp edges. Four node shell element with reduced integration (S4R) was used to generate the mesh. The mesh convergence study was done using the elastic critical buckling analysis for a range of mesh sizes, and the mesh size of twice the smallest thickness was adopted in the model. The elastic critical buckling load obtained from the GBTUL was used to validate the numerical model. Further, the nonlinear analysis was done for all parameters mentioned in 12 sets. The first mode shape obtained from the elastic critical buckling analysis was used as the initial geometrical imperfection with an amplitude of 0.34 times the minimum thickness of the legs. The residual stress developed within the member was not accounted for in this study since the detailed residual stress distribution for the 3D LPBF printed angle members was not available. The finite element results are presented in Table 3. The specimens are named, for example, 40×50×0.80×1.00. It is in the form of ($b_1 \times b_2 \times t_1 \times t_2$) where b_1 and b_2 are the element widths of the centerline dimension; t_1 and t_2 are the element thickness. The (b_1/t_1) and (b_2/t_2) are the element slenderness ratios of elements 1 and 2.

Table 2: Results

Sl. No	Specimen	b_1/t_1	b_2/t_2	σ_{crl} (MPa)	σ_{crc} (MPa)	λ_l	λ_c	$\sigma_{u\text{FE}}$ (MPa)	σ_{nc} (MPa)	σ_{nl} (MPa)	$\sigma_{u\_\text{FE}}/\sigma_{nl}$
1	40×40×0.8	49.5	49.5	86.6	57.2	0.8	3.1	182.2	50.1	48.3	3.77
2	40×40×1.0	39.5	39.5	136.3	89.5	0.8	2.4	218.6	78.5	75.6	2.89
3	40×40×1.2	32.8	32.8	196.9	129.0	0.8	2.0	247.9	113.1	109.1	2.27

4	40×40×1.6	24.5	24.5	353.6	230.0	0.8	1.5	292.6	201.7	194.7	1.50
5	40×40×1.8	21.7	21.7	449.8	291.5	0.7	1.4	312.9	248.2	241.1	1.30
6	40×40×2.0	19.5	19.5	558.2	360.3	0.7	1.2	333.4	287.4	282.6	1.18
7	40×40×3.0	12.8	12.8	1288.8	817.4	0.6	0.8	421.5	406.8	406.8	1.04
8	40×40×4.0	9.5	9.5	2353.0	1460.2	0.4	0.6	471.9	458.9	458.9	1.03
9	40×40×5.0	7.5	7.5	3773.2	2300.0	0.4	0.5	500.2	485.4	485.4	1.03
10	40×40×6.0	6.2	6.2	5582.5	3327.9	0.3	0.4	693.4	500.2	500.2	1.39
11	120×120×0.8	149.5	149.5	9.5	6.3	0.8	9.2	63.6	5.6	5.3	11.91
12	120×120×1.0	119.5	119.5	14.9	9.9	0.8	7.4	81.4	8.7	8.3	9.76
13	120×120×1.2	99.5	99.5	21.4	14.3	0.8	6.1	94.5	12.5	12.0	7.86
14	120×120×1.6	74.5	74.5	38.3	25.4	0.8	4.6	122.3	22.2	21.4	5.71
15	120×120×1.8	66.2	66.2	48.5	32.1	0.8	4.1	139.0	28.2	27.1	5.13
16	120×120×2.0	59.5	59.5	60.0	39.7	0.8	3.7	155.0	34.8	33.5	4.63
17	120×120×3.0	39.5	39.5	136.1	89.5	0.8	2.4	218.3	78.5	75.6	2.89
18	120×120×4.0	29.5	29.5	244.1	159.4	0.8	1.8	260.4	139.8	134.9	1.93
19	120×120×5.0	23.5	23.5	384.8	249.6	0.8	1.5	303.8	218.2	210.9	1.44
20	120×120×6.0	19.5	19.5	559.0	360.3	0.7	1.2	337.0	287.4	282.7	1.19
21	40×40×0.8×0.8	49.5	49.5	86.6	57.2	0.8	3.1	182.2	50.1	48.3	3.77
22	40×40×1.0×0.8	39.6	49.4	98.9	71.9	0.8	2.7	201.8	63.0	59.6	3.39
23	40×40×1.2×0.8	33.0	49.3	99.8	85.8	0.9	2.5	223.4	75.3	68.7	3.25
24	40×40×1.6×0.8	24.8	49.0	96.0	104.6	1.0	2.3	262.3	91.7	79.0	3.32
25	40×40×1.8×0.8	22.0	48.9	94.6	109.7	1.0	2.2	281.9	96.2	81.6	3.46
26	40×40×2.0×0.8	19.8	48.8	93.7	112.5	1.0	2.2	302.7	98.7	82.9	3.65
27	40×40×3.0×0.8	13.2	48.1	93.0	115.8	1.0	2.1	443.4	101.6	84.5	5.25
28	40×40×4.0×0.8	9.9	47.5	94.7	118.3	1.0	2.1	473.7	103.7	86.2	5.50
29	40×40×5.0×0.8	7.9	46.9	96.9	120.6	1.0	2.1	500.8	105.8	88.0	5.69
30	40×40×6.0×0.8	6.6	46.3	89.2	123.0	1.1	2.1	514.4	107.9	87.1	5.90
31	40×40×0.8×1.0	49.4	39.6	98.9	71.9	0.8	2.7	201.8	63.0	59.6	3.39
32	40×40×1.0×1.0	39.5	39.5	136.1	89.5	0.8	2.4	218.6	78.5	75.6	2.89
33	40×40×1.2×1.0	32.9	39.4	153.6	107.8	0.8	2.2	233.6	94.6	90.0	2.60
34	40×40×1.6×1.0	24.7	39.2	156.0	142.3	0.9	1.9	269.7	124.8	112.3	2.40
35	40×40×1.8×1.0	21.9	39.1	153.6	155.1	0.9	1.9	287.7	136.0	119.5	2.41
36	40×40×2.0×1.0	19.8	39.0	151.3	164.6	1.0	1.8	303.6	144.4	124.5	2.44
37	40×40×3.0×1.0	13.2	38.5	147.3	179.8	1.0	1.7	431.8	157.7	131.9	3.27
38	40×40×4.0×1.0	9.9	38.0	148.8	184.1	1.0	1.7	473.2	161.5	134.5	3.52
39	40×40×5.0×1.0	7.9	37.5	151.8	187.9	1.0	1.7	497.8	164.8	137.3	3.63
40	40×40×6.0×1.0	6.6	37.0	155.6	191.7	1.0	1.7	512.1	168.2	140.2	3.65
41	40×40×0.8×1.2	49.3	33.0	99.8	85.8	0.9	2.5	223.4	75.3	68.7	3.25
42	40×40×1.0×1.2	39.4	32.9	153.6	107.8	0.8	2.2	233.6	94.6	90.0	2.60
43	40×40×1.2×1.2	32.8	32.8	196.9	129.0	0.8	2.0	247.9	113.1	109.1	2.27
44	40×40×1.6×1.2	24.6	32.7	227.5	173.4	0.8	1.8	277.9	152.1	142.4	1.95

45	40×40×1.8×1.2	21.9	32.6	227.6	194.4	0.9	1.7	292.7	170.5	155.8	1.88
46	40×40×2.0×1.2	19.7	32.5	225.2	212.6	0.9	1.6	308.1	186.4	166.5	1.85
47	40×40×3.0×1.2	13.1	32.1	215.9	256.6	1.0	1.4	431.1	223.6	188.6	2.29
48	40×40×4.0×1.2	9.9	31.7	216.0	263.9	1.0	1.4	475.9	229.0	192.0	2.48
49	40×40×5.0×1.2	7.9	31.3	219.5	269.8	1.0	1.4	495.0	233.3	195.4	2.53
50	40×40×6.0×1.2	6.6	30.8	224.5	275.4	1.0	1.4	508.2	237.3	199.1	2.55
51	40×20×0.80×0.39	49.8	49.8	82.1	55.0	0.8	3.1	178.5	48.3	46.3	3.85
52	40×25×1.00×0.62	39.7	39.7	129.1	84.7	0.8	2.5	219.5	74.3	71.6	3.06
53	40×30×1.20×0.89	33.0	33.0	186.9	120.3	0.8	2.1	248.1	105.5	102.1	2.43
54	40×35×1.60×1.39	24.6	24.6	346.4	217.8	0.7	1.6	286.7	191.0	185.6	1.54
55	40×40×1.80×1.80	21.7	21.7	449.8	291.5	0.7	1.4	312.9	248.2	241.1	1.30
56	40×45×2.00×2.26	19.4	19.4	555.0	346.1	0.7	1.2	335.0	280.1	276.4	1.21
57	40×50×3.00×3.82	12.7	12.7	1271.3	786.4	0.6	0.8	425.4	402.4	402.4	1.06
58	40×55×4.00×5.71	9.3	9.3	2339.5	1435.2	0.4	0.6	486.4	457.7	457.7	1.06
59	40×60×5.00×7.98	7.2	7.2	3872.7	2312.5	0.4	0.5	514.5	485.6	485.6	1.06
60	40×65×6.00×10.74	5.8	5.8	6049.6	3410.8	0.3	0.4	524.0	501.0	501.0	1.05
61	40×20×0.80×0.39	49.8	49.8	82.1	55.0	0.8	3.1	178.5	48.3	46.3	3.85
62	40×25×0.80×0.50	49.7	49.7	81.4	54.4	0.8	3.1	182.5	47.7	45.8	3.98
63	40×30×0.80×0.60	49.6	49.6	82.5	53.8	0.8	3.2	182.7	47.2	45.5	4.01
64	40×35×0.80×0.70	49.6	49.6	85.1	54.6	0.7	3.1	182.3	47.8	46.3	3.94
65	40×40×0.80×0.80	49.5	49.5	86.6	57.2	0.8	3.1	182.2	50.1	48.3	3.77
66	40×45×0.80×0.90	49.4	49.4	85.8	54.6	0.7	3.1	181.8	47.9	46.4	3.91
67	40×50×0.80×1.00	49.4	49.4	84.3	53.6	0.7	3.2	180.3	47.0	45.6	3.95
68	40×55×0.80×1.11	49.3	49.3	83.2	54.6	0.8	3.1	183.7	47.8	46.1	3.98
69	40×60×0.80×1.21	49.2	49.2	82.9	54.7	0.8	3.1	183.6	48.0	46.2	3.98
70	40×65×0.80×1.31	49.2	49.2	83.1	54.9	0.8	3.1	182.3	48.2	46.4	3.93
71	40×20×1.60×0.78	24.8	24.8	332.3	219.8	0.8	1.6	290.5	192.8	185.5	1.57
72	40×25×1.60×0.98	24.7	24.7	329.4	216.2	0.8	1.6	293.4	189.6	182.8	1.60
73	40×30×1.60×1.19	24.6	24.6	334.7	215.0	0.8	1.6	294.8	188.6	182.5	1.62
74	40×35×1.60×1.39	24.6	24.6	346.4	217.8	0.7	1.6	286.7	191.0	185.6	1.54
75	40×40×1.60×1.60	24.5	24.5	353.6	230.0	0.8	1.5	292.6	201.7	194.8	1.50
76	40×45×1.60×1.81	24.4	24.4	351.1	221.5	0.7	1.6	295.5	194.3	188.6	1.57
77	40×50×1.60×2.02	24.4	24.4	345.6	219.4	0.7	1.6	296.4	192.4	186.6	1.59
78	40×55×1.60×2.23	24.3	24.3	342.4	220.3	0.8	1.6	294.4	193.2	186.9	1.57
79	40×60×1.60×2.44	24.2	24.2	342.1	222.3	0.8	1.6	296.7	195.0	188.3	1.58
80	40×65×1.60×2.66	24.2	24.2	343.9	226.7	0.8	1.5	299.0	198.8	191.5	1.56
81	40×20×3.00×1.41	13.1	13.1	1188.9	753.6	0.6	0.8	434.8	397.5	397.5	1.09
82	40×25×3.00×1.80	13.0	13.0	1183.4	753.7	0.6	0.8	432.2	397.5	397.5	1.09
83	40×30×3.00×2.20	13.0	13.0	1205.6	754.6	0.6	0.8	425.0	397.6	397.6	1.07
84	40×35×3.00×2.60	12.9	12.9	1254.6	772.4	0.6	0.8	420.8	400.4	400.4	1.05
85	40×40×3.00×3.00	12.8	12.8	1288.8	817.4	0.6	0.8	421.5	406.8	406.8	1.04

86	40×45×3.00×3.41	12.8	12.8	1285.4	790.5	0.6	0.8	421.2	403.0	403.0	1.05
87	40×50×3.00×3.82	12.7	12.7	1271.3	786.4	0.6	0.8	425.4	402.4	402.4	1.06
88	40×55×3.00×4.24	12.6	12.6	1266.8	795.6	0.6	0.8	432.8	403.8	403.8	1.07
89	40×60×3.00×4.66	12.6	12.6	1274.0	807.5	0.6	0.8	438.3	405.4	405.4	1.08
90	40×65×3.00×5.09	12.5	12.5	1289.6	822.0	0.6	0.8	442.5	407.4	407.4	1.09
91	40×40×0.80×0.80	49.5	49.5	86.6	57.2	0.8	3.1	182.2	50.1	48.3	3.77
92	40×50×0.80×1.00	49.4	49.4	84.3	54.2	0.8	3.1	181.0	47.5	46.0	3.94
93	40×60×0.80×1.20	49.3	49.3	82.9	54.7	0.8	3.1	183.9	48.0	46.2	3.98
94	40×79×0.80×1.60	49.0	49.0	84.6	56.8	0.8	3.1	182.8	49.8	47.8	3.82
95	40×88×0.80×1.80	48.9	48.9	85.8	57.6	0.8	3.0	180.8	50.5	48.5	3.73
96	40×98×0.80×2.00	48.8	48.8	86.9	58.2	0.8	3.0	176.9	51.1	49.0	3.61
97	40×145×0.80×3.00	48.1	48.1	90.9	59.8	0.8	3.0	134.7	52.5	50.5	2.67
98	40×190×0.80×4.00	47.5	47.5	93.9	60.3	0.8	3.0	91.5	52.8	51.1	1.79
99	40×235×0.80×5.00	46.9	46.9	96.6	59.4	0.7	3.0	70.0	52.1	50.8	1.38
100	40×278×0.80×6.00	46.3	46.3	99.4	57.2	0.7	3.1	62.9	50.2	49.5	1.27
101	40×21×1.60×0.80	24.8	24.8	331.4	219.1	0.8	1.6	291.1	192.2	185.0	1.57
102	40×25×1.60×1.00	24.7	24.7	329.6	215.9	0.8	1.6	293.5	189.3	182.6	1.61
103	40×30×1.60×1.20	24.6	24.6	335.4	214.5	0.7	1.6	294.1	188.1	182.2	1.61
104	40×40×1.60×1.60	24.5	24.5	353.6	230.0	0.8	1.5	292.6	201.7	194.8	1.50
105	40×45×1.60×1.80	24.4	24.4	351.4	221.5	0.7	1.6	295.1	194.3	188.6	1.56
106	40×50×1.60×2.00	24.4	24.4	346.1	219.2	0.7	1.6	295.9	192.2	186.5	1.59
107	40×73×1.60×3.00	24.1	24.1	349.1	230.4	0.8	1.5	296.5	202.1	194.6	1.52
108	40×96×1.60×4.00	23.8	23.8	366.0	239.7	0.8	1.5	289.2	210.2	202.7	1.43
109	40×118×1.60×5.00	23.4	23.4	380.6	244.4	0.7	1.5	270.4	214.0	207.2	1.31
110	40×140×1.60×6.00	23.1	23.1	393.6	246.0	0.7	1.5	249.9	215.3	209.4	1.19
111	40×12×3.00×0.80	13.2	13.2	1208.6	674.4	0.6	0.9	401.5	383.8	383.8	1.05
112	40×15×3.00×1.00	13.2	13.2	1203.6	722.8	0.6	0.9	420.4	392.5	392.5	1.07
113	40×17×3.00×1.20	13.1	13.1	1197.7	744.8	0.6	0.8	430.6	396.1	396.1	1.09
114	40×22×3.00×1.60	13.1	13.1	1183.6	755.6	0.6	0.8	435.1	397.8	397.8	1.09
115	40×25×3.00×1.80	13.0	13.0	1183.5	754.4	0.6	0.8	432.5	397.6	397.6	1.09
116	40×28×3.00×2.00	13.0	13.0	1189.9	752.7	0.6	0.8	428.7	397.3	397.3	1.08
117	40×40×3.00×3.00	12.8	12.8	1288.8	817.4	0.6	0.8	421.5	406.8	406.8	1.04
118	40×52×3.00×4.00	12.7	12.7	1267.7	789.2	0.6	0.8	428.7	402.8	402.8	1.06
119	40×64×3.00×5.00	12.5	12.5	1286.0	818.1	0.6	0.8	441.5	406.9	406.9	1.09
120	40×76×3.00×6.00	12.3	12.3	1334.6	845.3	0.6	0.8	445.4	410.5	410.5	1.09

5. Direct Strength Method

The nominal axial strength (P_{nl}) incorporating the local-global buckling interaction was evaluated using Eq. 1 – 4 as per AISI-S100-2024, clause E3.2. The equations presented below, σ_{crl} is the elastic critical local buckling stress ($\sigma_{crl} = P_{crl}/A$), P_{crl} is obtained from the signature curve plotted using GBTUL by forcing the involved modes as local, and A is the area of the cross-section. σ_{crc}

or F_{cre} ($\sigma_{crc} = F_{cre} = P_{cre}/A$) is the elastic critical global buckling stress determined using the elastic buckling load (P_{cre}) obtained from the finite element model for the actual (fixed-fixed) support condition. σ_{nc} or F_n is the global buckling compressive stress, $P_{ne} = F_n \times A$, σ_{nl} is nominal axial stress ($\sigma_{nl} = P_{nl}/A$), and F_y is the yield stress (534.93 N/mm^2). Since the results for compression are already conservative, as shown in Table 2, the interaction between flexure and compression mentioned in clause H1.2 is not accounted for in the calculations.

$$P_{nl} = 1.2P_{ne}\left(\frac{1 + 0.10\lambda_l^2}{1 + 0.55\lambda_l^2}\right) \leq P_{ne} \quad for\ \lambda_l \leq 5 \tag{1}$$

$$\lambda_l = \sqrt{\frac{P_{ne}}{P_{crl}}} \tag{2}$$

$$F_n = \left(0.658^{\lambda_c^2}\right)F_y \quad for\ \lambda_c \leq 1.5 \tag{3}$$

$$F_n = \left(\frac{0.877}{\lambda_c^2}\right)F_y \quad for\ \lambda_c > 1.5 \tag{4}$$

$$\lambda_c = \sqrt{\frac{F_y}{F_{cre}}}$$

6. Results and Discussion

Sets 1 and 2 have equal width for both elements; however, the set 2 element width is three times that of the set 1 element. The element thickness was maintained the same for both sets. Hence, set 2 cross-section elements are very slender, resulting in relatively lower elastic buckling and ultimate strength. The element slenderness associated with the 6 mm thick specimen in set 2 and the 2 mm thick specimen in set 1 exhibits similar behavior, emphasizing that equal element slenderness with a constant non-dimensional slenderness ratio results in the same capacity. That is, there is no size effect, and hence 40×40×2 and 120×120×6 angles behave similarly. The scale factor of 3 in set 2 geometry is reflected in the specimens' elastic critical pure local buckling capacity, which is 9 times lower than that of the first set of respective specimens. It implies that the size effect does not influence the inter-element interaction, but it directly reflects on element slenderness. In FE results, the interaction of the global mode is reflected, and hence it is lower than the pure local buckling predictions of the DSM results as shown in Fig. 2 (a).

Set 3-5, the non-dimensional slenderness ratio of the member does not vary significantly; however, the ultimate strength varies significantly. Hence, a single DSM curve will not be sufficient for the strength prediction. The strength prediction equation is also influenced by inter-element interactions when the element slendernesses differ. As the nonslenderness in one element increases, the ultimate strength of the slender angle increases, indicating the clear contribution of the non-slender element in ultimate capacity. It is also observed that the failure mode of these sets starts with the torsional mode in set 3 and ends with the local mode in set 5. For the non-slender and slender element angle section, the capacity is not much influenced by the slenderness of the slender element. In contrast, the non-slender element contribution is similar for all three sets.

Set 6 specimens are comparable with set 1 specimens, as the element slenderness ratio is the same for both sets. However, the change in thickness for the set 6 samples is not sensitive until it matches the same width and thickness (40×1.8 mm) for both elements. When the thickness increases higher than the other element thickness due to increased width, the inter-element interaction is noticeable.

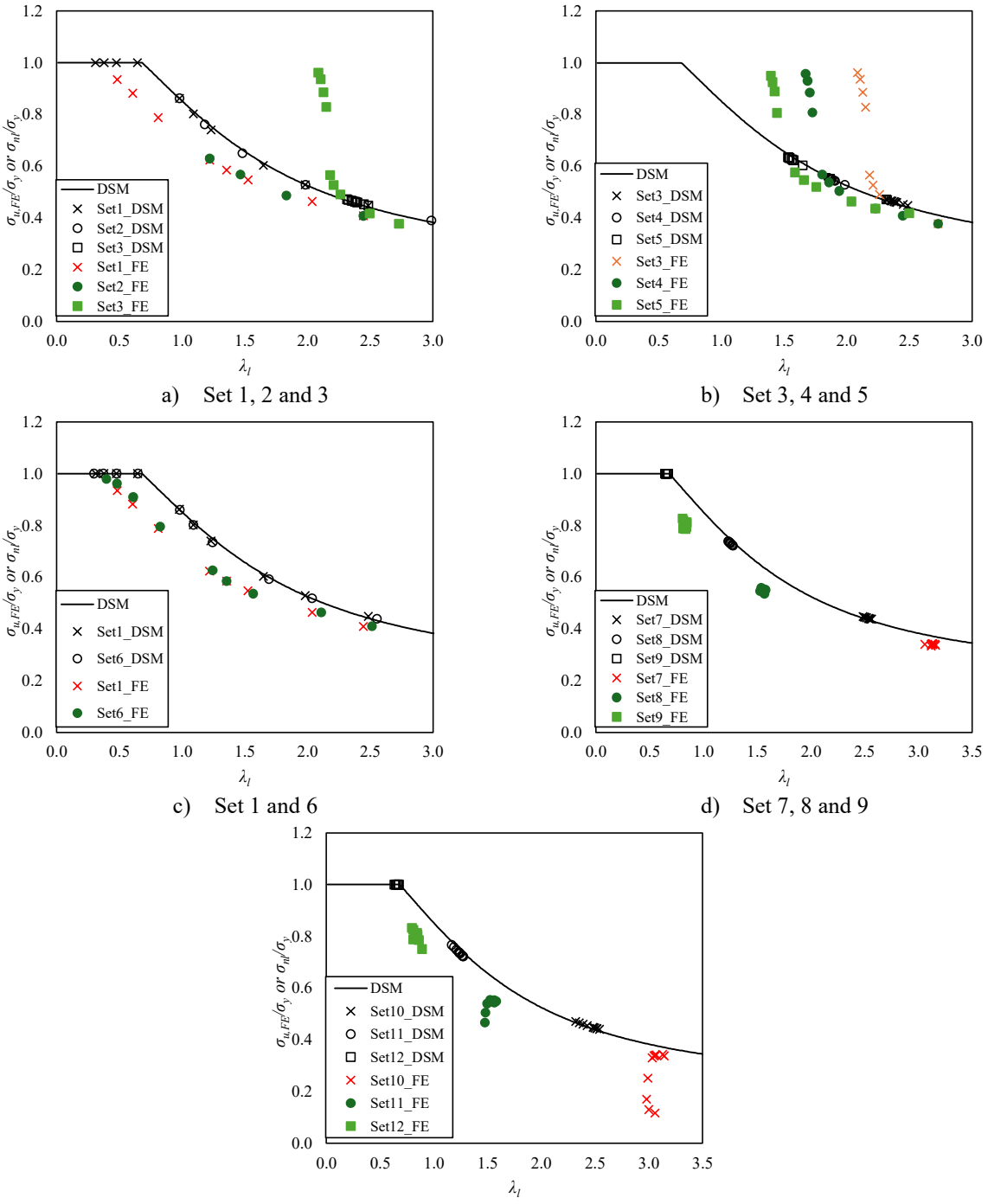

a) Set 1, 2 and 3

b) Set 3, 4 and 5

c) Set 1 and 6

d) Set 7, 8 and 9

e) Set 10, 11 and 12

Figure 2: DSM and FE results comparison

Set 7-9, the slenderness of the elements is constant, that is, equal within the elements and their respective set. The results show that the non-dimensional slenderness ratio remains constant even though the thickness of one element is varied to match the same slenderness for the respective varied element width. It can be concluded that the element slenderness mainly determines the simultaneous buckling. The independent effect of width or thickness is not prominent in buckling or ultimate strength for slender angles with equal slenderness in both elements. Post-buckling strength is prominent for very slender sections. A single strength curve shall be sufficient to estimate the nominal strength. Comparing these results with set 6 specimens, it can be deduced that the element thickness is significant when one of the elements is non-slender.

Set 10-12, the slenderness of the elements is constant, that is, equal within the elements and their respective set. The results show that the non-dimensional slenderness ratio remains constant even though the thickness and respective flange dimensions are varied for one element to match the same slenderness of another element of constant width and thickness. However, the ultimate capacity of the members rapidly decreases for the higher element slenderness sections (set 10) as the width and thickness increases even though the element slenderness and non-dimensional slenderness ratio are maintained. It shows that the post-buckling strength depends on the aspect ratio and the thickness. At the same time, set 12 shows an increasing ultimate capacity with increasing element width and thickness. Hence, the element's aspect ratio and thickness vary nonlinearly. All specimens failed predominantly in torsional or FTB mode. No local buckling is observed.

The DSM predictions are conservative for the sections. The DSM equations are developed for the mild steel sections and evaluated for the austenitic stainless steel grade of 316L. Although the articles [Zhang. L, et al., 2020a, Zhang. L, et al., 2020b, Zhang. L, et al., 2021, Zhang. L, et al., 2023] state that the DSM results perform relatively well, they may be unconservative in some cases. However, our results are obtained for the LPBF 3D-printed 316L grade, which has entirely different yield and ultimate strength compared to the traditional austenitic 316L grade, and hence the post-buckling strength is significantly influenced.

4. Conclusions

The cold-formed steel sections have uniform thickness across all elements, since they are fabricated from sheet. The DSM design is well demonstrated for cold-formed steel members. However, thin-walled members fabricated by welding plate elements of different thicknesses can have capacities that differ from the DSM predictions. Hence, extending the applicability of DSM to thin-walled members needs a thorough understanding of inter-element interactions and material properties of the plate elements. To assess the influence of element geometry, 3D metal printing was used to produce elements of different thicknesses while maintaining the same material properties.

In this study, angle sections composed of two unstiffened elements were numerically analyzed to understand their buckling behavior for various element slendernesses. Thicknesses of the elements and/or widths of the elements were maintained as different within the cross-section while maintaining the same element slenderness. It is observed that inter-element interaction is affected for equal slender but unequal angles, and DSM needs improvement to incorporate these inferences.

References

Arrayago, I., Real, E. and Gardner, L. (2015) "Description of stress-strain curves for stainless steel alloys." *Materials and Design*, 87, pp. 540–552. https://doi.org/10.1016/j.matdes.2015.08.001.

Buchanan, C., Matilainen. V., Salmine, A., and Gardner, L., (2017) "Structural performance of additive manufactured metallic material and cross-sections," *Journal of Constructional Steel Research*, 136, pp. 35–48. https://doi.org/10.1016/j.jcsr.2017.05.002.

Chen, X., Zhao, O., Xu. F, Zhi, J., and Sun, Y., (2025) "Cross-Sectional Capacity of Wire Arc Additively Manufactured Stainless Steel Channel Section Stub Columns," *Journal of Structural Engineering*, 151(6). DOI: https://doi.org/10.1061/jsendh.steng-14194.

Chepkoech, M., Owolabi, G. and Warner, G. (2024) "Investigation of Microstructures and Tensile Properties of 316L Stainless Steel Fabricated via Laser Powder Bed Fusion," *Materials*, 17(4). DOI: https://doi.org/10.3390/ma17040913.

Evans, S.I., Hadjipantelis, N. and Wang, J. (2024) "Stub column tests on wire arc additively manufactured equal-leg angle sections," *Engineering Structures*, 317. https://doi.org/10.1016/j.engstruct.2024.118591.

Evans, S.I., Xu, F. and Wang, J. (2023) "Material properties and local stability of WAAM stainless steel equal angle sections," *Engineering Structures*, 287. DOI: https://doi.org/10.1016/j.engstruct.2023.116160.

Francis, R., Shabhari, A., Chandrasekar, D., and Vijaya Vengadesh Kumar, J. (2024) "Investigation of local buckling behavior of web perforated plain channel stub columns," *Journal of Constructional Steel Research*, 222. https://doi.org/10.1016/j.jcsr.2024.108978.

Francis, R., Shabhari, A., Vijaya Vengadesh Kumar, J. and Chandrasekar, D., (2025) "Local buckling strength enhancement due to non-slender flanges in web perforated plain channel columns," *Structures*, 82. https://doi.org/10.1016/j.istruc.2025.110507.

Gardner, L. (2023) "Metal additive manufacturing in structural engineering – review, advances, opportunities and outlook," *Structures*. Elsevier Ltd, pp. 2178–2193. https://doi.org/10.1016/j.istruc.2022.12.039.

Huang, C., Meng, X. and Gardner, L. (2022) "Cross-sectional behaviour of wire arc additively manufactured tubular beams," *Engineering Structures*, 272. https://doi.org/10.1016/j.engstruct.2022.114922.

Kumar, M. V. A., and Kalyanaraman, V. (2013). Design Strength of Locally Buckling Stub-Lipped Channel Columns. 138(11), 1291–1299. https://doi.org/10.1061/(ASCE)ST.1943-541X.0000575.

Mahar, A. M., Jayachandran, S. A., and Mahendran, M. (2021) "Direct Strength Method for Cold-Formed Steel Unlipped Channel Columns Subject to Local Buckling," *Int. J. Steel Struct*., vol. 21, no. 6, pp. 1977–1987, doi: 10.1007/s13296-021-00547-1.

Rasmussen, K. J. R. (2006) "Design of Slender Angle Section Beam-Columns by the Direct Strength Method." *Journal of Structural Engineering,* https://doi.org/10.1061/ASCE0733-94452006132:2204.

Shamsujjoha, M., Agnew, S. R., Fitz-Gerald, J. M., Moore, W. R., and Newman, T. A., (2018) "High Strength and Ductility of Additively Manufactured 316L Stainless Steel Explained," *Metallurgical and Materials Transactions A: Physical Metallurgy and Materials Science*, 49(7), pp. 3011–3027. https://doi.org/10.1007/s11661-018-4607-2.

Xu. M., Guo, H., Wang, Y., Hou, Y., Dong, Z., and Zhang, L., (2023) "Mechanical properties and microstructural characteristics of 316L stainless steel fabricated by laser powder bed fusion and binder jetting," *Journal of Materials Research and Technology*, 24, pp. 4427–4439.: https://doi.org/10.1016/j.jmrt.2023.04.069.

Yin Y. J., Sun J. Q., Guo, J., Kan, X. F., and Yang, D.C., (2019) "Mechanism of high yield strength and yield ratio of 316 L stainless steel by additive manufacturing," *Materials Science and Engineering: A*, 744, pp. 773–777. https://doi.org/10.1016/j.msea.2018.12.092.

Zhang, L., Liang, Y. and Zhao, O. (2020) "Experimental and numerical investigations of pin-ended hot-rolled stainless steel angle section columns failing by flexural buckling," *Thin-Walled Structures*, 156. https://doi.org/10.1016/j.tws.2020.106977.

Zhang, L., Liang, Y. and Zhao, O. (2020) "Flexural-torsional buckling behaviour and resistances of fixed-ended press-braked S690 high strength steel angle section columns," *Engineering Structures*, 223. https://doi.org/10.1016/j.engstruct.2020.111180.

Zhang, L., Liang, Y. and Zhao, O. (2021) "Laboratory testing and numerical modelling of pin-ended hot-rolled stainless steel angle section columns failing by flexural-torsional buckling," *Thin-Walled Structures*, 161. https://doi.org/10.1016/j.tws.2020.107395.

Zhang, L., Zhong, Y. and Zhao, O. (2023) "Structural behaviour and design of press-braked S690 high strength steel angle section long columns," *Thin-Walled Structures*, 182. https://doi.org/10.1016/j.tws.2022.110251.